Geophysical Research Letters

RESEARCH LETTER

10.1029/2020GL091447

Key Points:

- Regressions on a key El Niño index underestimate El Niño's impact on US precipitation both in winter but especially in fall and spring
- El Niño's impact is found by assembling regressions of precipitation on the SST principal components constituting ENSO variability
- El Niño's impact on US fall-winter-spring precipitation is much larger than previously noted, raising prospects for year-round prediction

Correspondence to:

S. Nigam,
nigam@umd.edu

Citation:

Nigam, S., & Sengupta, A. (2021). The full extent of El Niño's precipitation influence on the United States and the Americas: The suboptimality of the Niño 3.4 SST index. *Geophysical Research Letters*, *48*, e2020GL091447. https://doi.org/10.1029/2020GL091447

Received 26 OCT 2020
Accepted 5 DEC 2020

The Full Extent of El Niño's Precipitation Influence on the United States and the Americas: The Suboptimality of the Niño 3.4 SST Index

Sumant Nigam[1,2], and Agniv Sengupta[1,3]

[1]Department of Atmospheric and Oceanic Science, University of Maryland, College Park, MD, USA, [2]Fulbright-Nehru Fellow, Indian Institute of Technology, Mandi, India, [3]Now at Jet Propulsion Laboratory, California Institute of Technology, Pasadena, CA, USA

Abstract Key features of El Niño's influence on North American winter precipitation are well-known but we show that this influence has, hitherto, been suboptimally characterized in winter, and especially in fall and spring. The suboptimality has arisen from the historical over-reliance on regressions on the Niño 3.4 SST index—a widely used marker of El Niño variability. We show that El Niño's full influence is obtained from assembling the regressions on the spatiotemporal modes constituting El Niño variability, rather than from regressions on an SST index keyed just to its mature phase (Niño 3.4 index). The notably different influence of central and eastern Pacific El Niños on Eastern Seaboard is documented. The full influence of El Niño on North American precipitation is shown to be substantially larger than previously recognized and pronounced not just in northern winter but even in fall and spring—enhancing prospects for year-round seasonal prediction.

Plain Language Summary El Niño Southern Oscillation—a leading mode of year-to-year variability in the tropical Pacific Ocean—strongly influences the hydroclimate of adjacent continents. Scoping out its seasonal influence on North American precipitation—a potentially predictable influence because of El Niño's multiyear timescale—is the analysis goal. El Niño's influence is scoped out from analyses of century-long sea surface temperature and precipitation records as realistic representations of regional hydroclimate variability still elude climate system models. It is shown that linear regressions on a key El Niño index—a widely used method for extracting El Niño's influence—underestimates its influence on North American precipitation both in winter but especially in adjoining fall and spring. El Niño's full influence on precipitation is scoped out by assembling regressions of precipitation on the four SST principal components constituting El Niño variability. El Niño's full impact on US precipitation is shown to be more substantial than its earlier fall-to-spring portrayals, raising prospects for year-round seasonal prediction.

1. Introduction

Sea Surface Temperature (SST) exerts a significant, and often predictable, influence on Earth's climate. A notably influential mode of interannual SST variability is El Niño Southern Oscillation (ENSO) which is rooted in the tropical Pacific but whose hydroclimate impacts extend from South Asia in the west (Rasmusson & Carpenter, 1983) to North America in the east (e.g., Ropelewski & Halpert, 1987; Nigam, 2003; Joseph & Nigam, 2006; Nigam & Baxter, 2015); ENSO also influences Central and South American precipitation (Ropelewski & Halpert, 1987; Aceituno, 1988).

ENSO variability is rich, with individual El Niño episodes exhibiting interesting differences, or flavors (e.g., Capotondi et al., 2015). The rich spectrum of ENSO variability is a manifestation of the multiple recurrent spatiotemporal structures (or modes) of variability constituting ENSO and their mutual lead-lags. Guan and Nigam (2008) identified four underlying modes—ENSO-Growth and ENSO-Decay, representing canonical ENSO variability (*aka* Eastern Pacific El Niño); ENSO-Noncanonical (*aka* Central Pacific El Niño or El Niño Modoki); and Biennial variability—from an extended-EOF analysis of seasonal SST anomalies in a century-long (1900–2002) record. ENSO's complex spatiotemporal evolution was also noted by Compo and Sardeshmukh (2010) who cautioned against its filtering using just the Niño 3.4 SST index, implicitly referring to the incomplete capture of ENSO variability by this index.

Guan and Nigam (2008, section 3c) showed that a *synthetic* Niño 3.4 SST index, i.e., one constructed using SST regressions on the principal components of the four constituent modes of ENSO, is highly correlated (~0.95) with the *observed* Niño 3.4 SST index in the century-long record. Even so, resolving the constituent modes is imperative for the full characterization of El Niño's near and far-field impacts, we show. The case is made from the comparison of the observed, composited El Niño precipitation anomalies at various stages of El Niño evolution with two reconstructions of the precipitation anomalies: The first is based on regressions of precipitation on the four constituent SST principal components in the century-long analysis period while the second on regressions on the observed Niño3.4 SST index.

Datasets and analysis methods are described in Section 2. Principal components constituting ENSO and their relationship with the Niño 3.4 SST index are discussed in Section 3, along with the efficacy of synthetic Niño 3.4 indices in representing ENSO. Seasonal precipitation anomalies over the Americas composited across four notable recent El Niño episodes, and their various reconstructions are in Section 4. Differences between the canonical and noncanonical El Niño precipitation anomalies are noted in Section 5, with concluding remarks following in Section 6.

2. Datasets and Analysis Method

2.1. Sea Surface Temperature

The UK Met Office's Hadley Center Sea Ice and Sea Surface Temperature data (HadISST 1.1; Rayner et al., 2003), available from 1900 to 2018 on a 1° grid, is analyzed. Seasonal anomalies are constructed by removing the long-term climatology of each season; likewise, for precipitation.

2.2. Niño 3.4 SST Index

The Niño 3.4 index is constructed from the 1° HadISST data, by the area-weighted averaging of SST anomalies in the central-eastern equatorial Pacific (170°W–120°W; 5°S–5°N; NOAA/ESRL). The same SST data and climatology reference is used in the subsequent principal component analysis.

2.3. SST Principal Components (PCs)

The SST PCs are obtained from an extended-EOF analysis of seasonal SST anomalies in a longitudinally global domain (20°S–80°N, 0–360°) for the period winter 1900—winter 2017/2018; a five-season-long sampling window is used in assessing spatiotemporal recurrence without imposing any periodicity constraints and data preprocessing conditions. Because of the focus on both spatial and temporal recurrence, the analysis yields recurrent modes (and not just patterns) of variability; specifically, a five-season-long spatiotemporal pattern (loading vector or extended-EOF) and its related time series (principal component). The evolution-centric SST analysis (Nigam et al., 2020) is similar to Guan and Nigam's (2008, 2009) but for the unfettered expression of Atlantic-Pacific basin interactions enabled by the longitudinally global analysis domain and analysis of a 15 years longer SST record. The evolution of SST (or any other variable) is obtained from the linear lead-lag regressions of their seasonal anomalies on the PCs.

In the interannual variability context—of interest here—four modes are obtained: ENSO-Growth and ENSO-Decay, representing canonical ENSO variability; ENSO-Noncanonical; and Biennial—all described in considerable detail in Guan and Nigam (2008; hereafter GN2008). The corresponding PCs in Nigam et al. (2020) are well-correlated (0.81–0.98) with those in GN2008 in the overlapping analysis period (1900–2002), especially canonical ones (both 0.98). [The same SST analysis also yields characterization of secular warming through a nonstationary trend, as well as multidecadal SST variability; a contextual separation, essential for detection and attribution of climate change.]

2.4. Precipitation

The Global Precipitation Climatology Center (GPCC; Becker et al., 2013) provides a monthly analysis of precipitation from quality-controlled rain gauge data. GPCC's Full Data Reanalysis Version eight data, available on a 0.5° continental grid from January 1901 to December 2016, is used in the construction of composited anomalies and for regressions on the SST principal components.

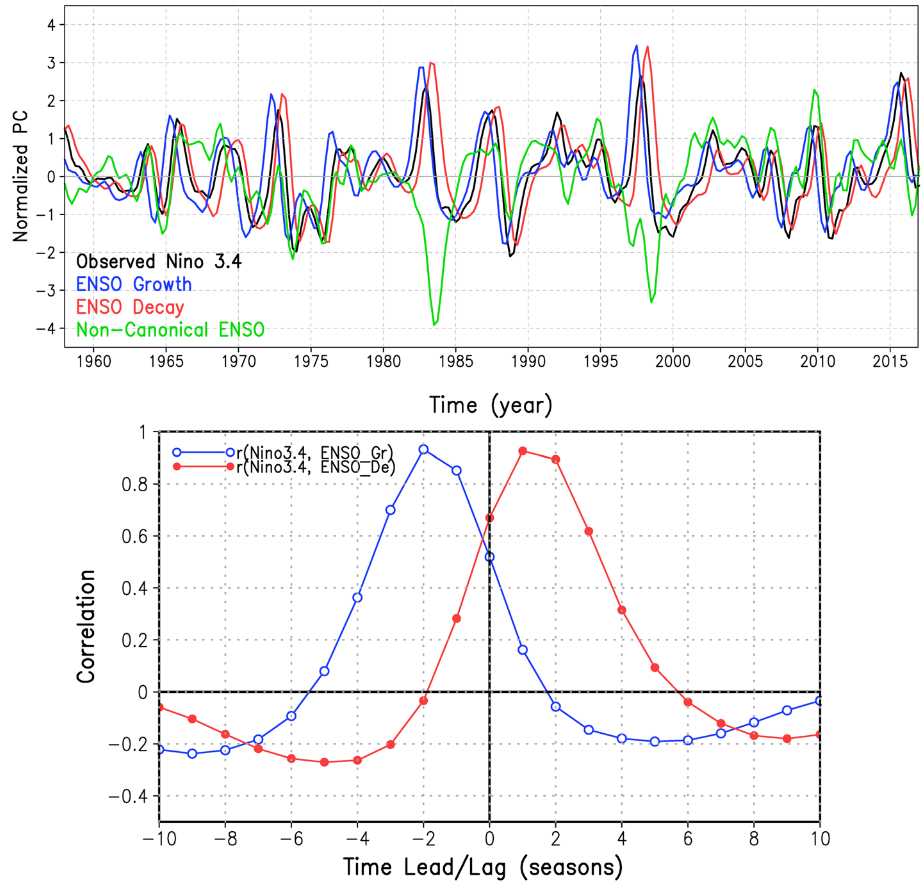

Figure 1. The three leading Principal Components (PCs) of ENSO SST variability—ENSO-Growth, ENSO-Decay, and ENSO-Noncanonical—and the Niño 3.4 SST index are shown at seasonal resolution (top). The PCs are obtained from an extended-EOF analysis of seasonal SST anomalies during 1900–2018 (Nigam et al., 2020). PCs and the Niño-3.4 SST index are normalized, smoothed (2 times 1-2-1), and shown in the post-1958 period for reasons of clarity. Cross correlations of the *un*smoothed ENSO PCs and Niño-3.4 index at various seasonal leads/lags are shown in the lower panel. The cross correlations, computed for the 1900–2016 period, indicate that ENSO-Growth PC leads the Niño-3.4 index by two seasons (blue) while the ENSO-Decay PC lags the index by 1–2 seasons (red). Note, correlations larger than ±0.19 are statistically significant at the 95% confidence level, as assessed by a two-tailed Student's *t* test. ENSO, El Niño Southern Oscillation; SST, Sea Surface Temperature.

3. SST Principal Components and the Niño 3.4 SST Index

The ENSO-Growth and ENSO-Decay PCs constituting canonical ENSO variability are shown with the Niño 3.4 index in Figure 1. The temporal lead of the former and the lag of the latter vis-à-vis this index is visually apparent and quantitatively confirmed from lead-lag correlations (lower panel): ENSO-Growth leads by two seasons while ENSO-Decay lags by 1–2 seasons, with both correlations exceeding 0.9; the two PCs are, of course, uncorrelated at zero-lag, as mandated by EOF analysis. Their mutual lead-lag correlations, shown in GN2008 (Figure 4), indicate that ENSO-Growth leads ENSO-Decay by 3–4 seasons, much as surmised from their lead-lags relative to the Niño 3.4 index. The ENSO-Noncanonical PC (green) however shows no systematic phase relationship with the canonical PCs.

3.1. Synthetic Niño 3.4 SST Index

The Niño 3.4 SST index is reconstructed from the spatiotemporal modes constituting ENSO variability. As this index is not computed directly from the observed SST anomalies, it is referred to as “synthetic.” The synthetic index is constructed as follows: The observed seasonal SST anomalies are first regressed on each SST PC over 1900–2016, yielding a temporally invariant SST anomaly pattern; this pattern is then multiplied by its time-var-

10.1029/2020GL091447

ying PC to yield this PC's contribution to the observed SST anomalies; the regression period ends in 2016 (and not 2018) as GPCC precipitation ends in 2016 (cf. Section 2.4). Various PC contributions can be summed and used in the computation of the Niño 3.4 SST index, following its standard definition (cf. Section 2.2), resulting in a synthetic Niño 3.4 SST index. The synthetic index can be based on SST anomaly contributions from the Canonical (two), Canonical + Biennial (three), or the Canonical + Biennial + Noncanonical (i.e., four) PCs.

The two-mode synthetic index based on canonical ENSO variability is correlated with the observed Niño 3.4 SST index at 0.847 while the three-mode index based on Canonical + Biennial variability is correlated at 0.869. The four-mode synthetic index, based on the full expression of ENSO variability in this spatiotemporal SST analysis, is correlated at 0.968! The high correlation indicates the efficacy of the extended-EOF analysis in extracting ENSO variability as well as relevance of the popular Niño 3.4 SST index as a marker of this variability.

Even so, the Niño 3.4 SST index is shown to be suboptimal in characterizing ENSO's precipitation influence (cf. Section 4).

4. Characterization of ENSO's Precipitation Influence

ENSO's full influence on seasonal precipitation over the Americas is characterized from analyses of century-long (1900–2016) SST and precipitation records. The observed precipitation anomalies composited over four strong recent El Niños (1972–1973, 1982–1983, 1997–1998, and 2015–2016) are the target of reconstruction, based on regressions of precipitation on the observed Niño 3.4 SST index and the ENSO-related SST PCs. Large-amplitude episodes enhance the signal-to-noise ratio in the composites; in each composited episode, at least two of the three SST PCs exceed 2 units (Figure 1, top panel). Large values of the ENSO-Growth and Decay PCs (and Niño 3.4 index) indicate significant canonical evolution (i.e., east-to-west SST development in the eastern basin). But the Noncanonical ENSO PC, representing west-to-east development in the central-eastern basin, is also not small at these times (see also, Figure 1 in GN2008, Figure 6 in Kao and Yu, 2009, Figure 1 in Infanti and Kirtman, 2016, Table 1 in Zhang et al., 2020), indicating complex SST evolution, and thus, inconclusive episode classification in some cases.

4.1. The Observed Influence—The Reconstruction Target

El Niño's precipitation influence was first characterized via compositing (e.g., Ropelewski and Halpert, 1987), as here. The influence on *winter* precipitation is noted first because it is impressive. The key features of the winter influence are well-documented (e.g., Ropelewski and Halpert, 1987; Trenberth et al., 1998; Nigam and Baxter, 2015) but reiterated here to provide the context for evaluation of the reconstructions. The key features, manifest also in the observed composite here (Figure 2, middle row, right column), include above-normal precipitation over North America and below-normal rainfall over Central and northern South America (sans Venezuela and Colombia) in boreal winter. The North American influence is focused along the West Coast and over the central-southern Great Plains, Gulf Coast states, and Eastern Seaboard. The West Coast focus is over California and the Pacific Northwest where winter precipitation is larger by ~2 mm/day. Precipitation anomalies are ~0.8 mm/day over the southern Great Plains (Oklahoma, Arkansas) but larger over the Gulf Coast states (Louisiana, Mississippi, Alabama, Florida) and Eastern Seaboard (Georgia and Carolinas) where they exceed 1.2 mm/day. El Niño's influence is impressive, especially over California and the Eastern Seaboard where climatological winter precipitation is only ~3 mm/day (e.g., Nigam and Ruiz-Barradas, 2006).

4.2. The Reconstructed Influence—From Observed Niño 3.4 SST Index

El Niño's influence on precipitation is first reconstructed from the regressions of seasonal precipitation on the observed Niño 3.4 SST index. Both because El Niño's peak phase is in northern winter (leading to largest index values in that season) and to distinguish El Niño's impact between antecedent and subsequent seasons (e.g., El Niño-prior and El Niño-following summers), *lead-lag* regressions on the *winter* Niño 3.4 SST index were computed in the 1901–2016 period. The seasonally resolved but otherwise temporally invariant precipitation regressions were multiplied by the time-varying winter Niño 3.4 SST index to extract El Niño's influence in the observed precipitation record. The index-based winter precipitation anomalies composited across the four El Niño episodes, are shown in Figure 2 (middle row, left column).

10.1029/2020GL091447

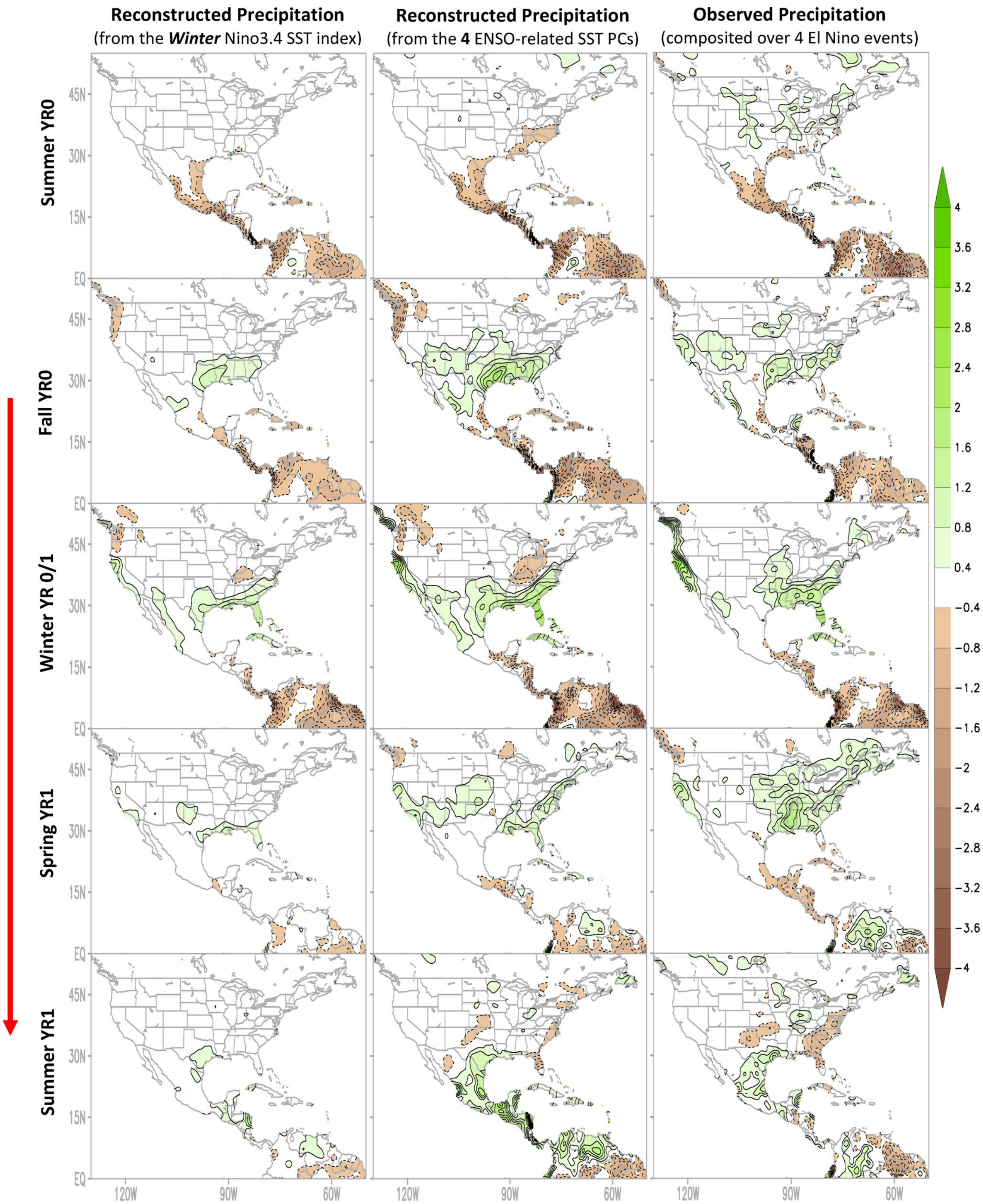

Comparison of the left and right panels in Figure 2 (middle row) shows the Niño 3.4 index-based winter precipitation anomalies to be broadly similar to the observed ones but for their weaker amplitude; the amplitude deficit is notable (∼50%) over northern California, Pacific Northwest, and the Eastern Seaboard. Another difference is the lack of penetration of the above-normal precipitation signal into the central Great Plains and the precipitation deficit over the lower Ohio Valley in the index-based reconstruction.

The discrepancy between the reconstructed and observed El Niño precipitation anomalies is even larger in the shoulder seasons of winter: In the preceding fall (Fall YR0; second row from top in Figure 2), the Niño 3.4 index-based reconstruction is devoid of the positive precipitation anomalies present over the western United States, including California. In the following spring (Spring YR1; second row from the bottom in Figure 2), the index-based reconstruction shows weak anomalies along the Gulf Coast and little elsewhere; in contrast, the observed anomalies are robust across large swaths of North America, especially the eastern half of the continent. Moving further away from the El Niño peak phase—to preceding and subsequent boreal summers—one again finds the Niño 3.4 index-based reconstruction of precipitation anomalies challenged given the absence of notable precipitation deficits (∼1 mm/day) over the Eastern Seaboard in the following summer's reconstruction (Summer YR1; bottom row in Figure 2).

El Niño's precipitation influence extracted from *contemporaneous* regressions on the Niño 3.4 SST index—a not uncommon approach (e.g., NOAA CPC)—is even more challenged in the shoulder seasons, especially the ones following winter. For example, surplus precipitation over the Gulf Coast in Spring of YR1 (cf. Figure 2, left column)—weakly reconstructed to begin with—is essentially missing in the reconstruction based on contemporaneous regressions (Appendix Figure A1). The winter anomalies in the two reconstructions—Figure 2 (left) and Appendix Figure A1—are, not surprisingly, identical.

4.3. The Reconstructed Influence—From ENSO-Related SST Principal Components

El Niño's precipitation influence is reconstructed again, this time, from regressions on the ENSO-related SST PCs. Contemporaneous regressions on the ENSO-Growth and Decay, Biennial, and ENSO-Noncanonical PCs during 1901–2016 constitute the building blocks—the temporally fixed patterns—which when multiplied by their temporally varying PCs and subsequently summed yield the ENSO precipitation anomaly in any year/season. The four-ENSO PC-based precipitation anomalies composited across four notable El Niño episodes are shown in Figure 2 (middle column). The large difference between the two reconstructions (left and middle columns) and the considerable similarity of the PC-based reconstruction with observations (middle and right columns) reveal the Niño 3.4 SST index's limited potential in yielding El Niño's precipitation influence in the context of this composite.

Notable differences in the index-based and PC-based reconstructions (left and middle column, Figure 2) include the large-amplitude discrepancy in winter (by a factor of 2?) and even larger differences in the shoulder seasons, e.g., North America is devoid of notable precipitation anomalies in spring and summer of YR1 in the index-based reconstruction (left column) but populated with fairly realistic anomalies in the PC-based one (middle). Intercomparison of the middle and right columns (Figure 2) shows many of the salient features of the observed precipitation anomalies during El Niño to be present in the four-PC-based reconstruction.

In summary, and in the context of this four-episode composite, the reconstruction of El Niño's precipitation influence during its growth, peak, and decay phases reveals that the Niño 3.4 SST index—perhaps, the most widely used marker of ENSO variability—is unable to extract the full influence of El Niño on American precipitation.

Figure 2. Reconstructed and Observed El Niño Precipitation Anomalies over the Americas, composited over four episodes (1972–1973, 1982–1983, 1997–1998, and 2015–2016): Reconstructed from lead-lag regressions on the Winter Niño 3.4 SST index (left); from contemporaneous regressions on the four ENSO-related SST principal components (PCs, middle); observed (right). Anomalies are relative to 1901–2016 which is also the regression period. Precipitation (GPCC v8; 0.5°) is contoured/shaded at interval and threshold of 0.4 mm/day after smoothing (2 × smth9 in GrADS). Seasonal anomalies are shown from the summer of YR0 (El Niño Growth year) to the summer of YR1 (El Niño Decay year), with time running downward. ENSO, El Niño Southern Oscillation; SST, Sea Surface Temperature; GPCC, Global Precipitation Climatology Center; PCs, Principal Components.

4.4. The Reconstructed Influence—A Conundrum

The large difference in the two reconstructions of El Niño's precipitation influence (Figure 2)—one from the observed Niño 3.4 SST index and the other from the four SST PCs constituting this index—pose a conundrum, especially, as the observed and the four-PC-based synthetic Niño 3.4 index are highly correlated (~0.97, section 3.1), generating an expectation of nearly identical reconstructions of El Niño's precipitation influence—an expectation not met (left and middle columns of Figure 2). The expectation is not met for the following reasons:

Consider a synthetic Niño 3.4 SST index, N34(t), based on just two SST principal components, $\mathrm{PC}_1(t)$ and $\mathrm{PC}_2(t)$; they, hypothetically, represent canonical ENSO variability, with PC_1 and PC_2 being the ENSO-Growth and ENSO-Decay PC, respectively (Section 3.1, Figure 1).

$$\mathrm{N34}(t) = \alpha\ \mathrm{PC}_1(t) + \beta \mathrm{PC}_2(t) \tag{1}$$

Normalization of N34(t) yields $\alpha^2+\beta^2 = 1$ for orthonormal PCs, i.e., $\sum_t \mathrm{PC}_i(t).\,\mathrm{PC}_j(t) = \delta_{i,j}$

Regressions of precipitation P(x,y,t) on the synthetic index are referred as RN34, and are

$$\mathrm{RN34}(x,y) = \frac{\sum_t \left[\alpha\ \mathrm{PC}_1(t) + \beta\ \mathrm{PC}_2(t)\right].\,\mathrm{P}(x,y,t)}{\sum_t \left[\mathrm{N34}(t).\,\mathrm{N34}(t)\right]} \tag{2}$$

As N34(t) is normalized, RN34(x,y) simplifies

$$\mathrm{RN34}(x,y) = \left[\alpha\ \mathrm{RPC}_1(x,y) + \beta\ \mathrm{RPC}_2(x,y)\right] \tag{3}$$

where RPC_1 [$= \sum_t \mathrm{PC}_1(t).\,\mathrm{P}(x,y,t)$] and RPC_2 (similarly defined) denote precipitation regressions on the SST principal components PC_1 and PC_2. Regressions of precipitation on the synthetic index are thus a weighted sum of the regressions on its constituent PCs.

The ENSO precipitation signal constructed from regressions of precipitation on the synthetic index is denoted by P_N34(x,y,t), and is simply

$$\begin{aligned}
\mathrm{P_N34}(x,y,t) &= \mathrm{N34}(t)\cdot\mathrm{RN34}(x,y)\\
&= \left[\alpha\ \mathrm{PC}_1(t) + \beta\ \mathrm{PC}_2(t)\right]\left[\alpha\ \mathrm{RPC}_1(x,y) + \beta\ \mathrm{RPC}_2(x,y)\right]\\
&= \alpha^2\mathrm{PC1}(t).\mathrm{RPC}_1(x,y) + \beta^2\mathrm{PC}_2(t).\mathrm{RPC}_2(x,y) + \alpha\beta\left[\mathrm{PC}_1(t).\mathrm{RPC}_2(x,y) + \mathrm{PC}_2(t).\mathrm{RPC}_1(x,y)\right]\\
&= \alpha^2\mathrm{P_PC}_1(x,y,t) + \beta^2\mathrm{P_PC}_2(x,y,t) + \alpha\beta\left[\text{cross terms}\right]
\end{aligned}$$

where $\mathrm{P\_PC}_1(x,y,t)$ is PC_1's contribution to the ENSO precipitation signal; likewise for $\mathrm{P\_PC}_2(x,y,t)$; the cross terms are products of PC with the other PC's precipitation regression.

In summary, in the context of two ENSO SST PCs and a Niño 3.4 SST index-based just on them (1), the *index-based* estimate of ENSO's precipitation influence is

$$\mathrm{P\_N34}(x,y,t) = \alpha^2\mathrm{P\_PC}_1(x,y,t) + \beta^2\mathrm{P\_PC}_2(x,y,t) + \alpha\beta\left[\text{cross terms}\right], \text{with } \alpha^2 + \beta^2 = 1 \tag{4}$$

while the *constituent PCs-based* estimate, denoted by P_PC(x,y,t), is

$$\mathrm{P\_PC}(x,y,t) = \mathrm{P\_PC}_1(x,y,t) + \mathrm{P\_PC}_2(x,y,t) \tag{5}$$

The index-based estimate of El Niño's precipitation influence (4) is thus *different* from the one based on its constituent SST PCs (5), both due to the weighting of the first two terms and the presence of the cross terms in Equation 4. *How different are the two estimates and which one is closer to El Niño's observed influence?*

An assessment follows in Figure 3 where the observed precipitation anomalies, composited over four recent El Niño episodes (shown earlier in Figure 2, right column), are reconstructed, this time, however from just

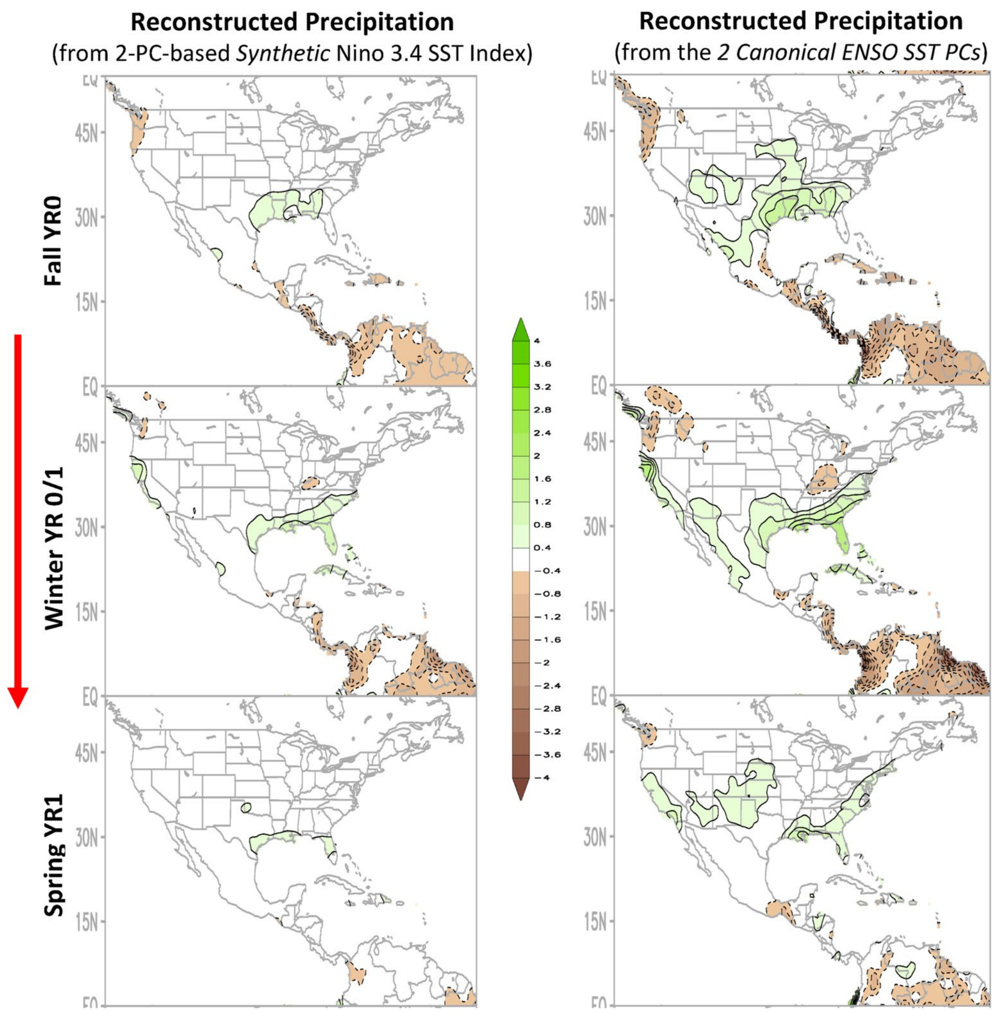

Figure 3. Reconstructed El Niño Precipitation Anomalies over the Americas, composited over four episodes (1972–1973, 1982–1983, 1997–1998, and 2015–2016): From contemporaneous regressions on the two Canonical ENSO PCs (Growth and Decay; Right), and on these two-PC-based Synthetic Niño 3.4 SST index (left). GPCC (v8) precipitation is regressed and contoured/shaded at interval and threshold of 0.4 mm/day. Rest as in Figure 2, including the regression period, 1901–2016. ENSO, El Niño Southern Oscillation; SST, Sea Surface Temperature; GPCC, Global Precipitation Climatology Center; PCs, Principal Components.

the two Canonical ENSO SST PCs (representing PC_1 and PC_2 above) and, for exact comparison, also from the synthetic Niño 3.4 SST index based on just these two PCs (cf. Section 3.1; representing N34 above). The synthetic index-based El Niño precipitation anomalies (Figure 3, left) are anemic vis-à-vis the PC-based ones (Figure 3, right), especially in the shoulder seasons, much as in Figure 2. A comparison of both reconstructions (Figure 3) with the observed precipitation anomalies (Figure 2, right)—the reconstruction target—shows that the two-PC-based reconstruction (Equation 5) is decidedly more realistic—that is, more optimal—than the index-based one (Equation 4), and not just in the shoulder seasons but in winter as well; answering the question posed at the beginning of the paragraph.

5. El Niño's Precipitation Impact: Canonical (E-Pacific) Versus Noncanonical (C-Pacific)

El Niño variability is rich, in part, from the varying relative contributions of its constituent modes, of which Canonical and Noncanonical ones are key (cf. Section 1). Their characteristic influence on US precipitation is documented in Figure 4 over a multiseason period centered on boreal winter, the El Niño peak-phase

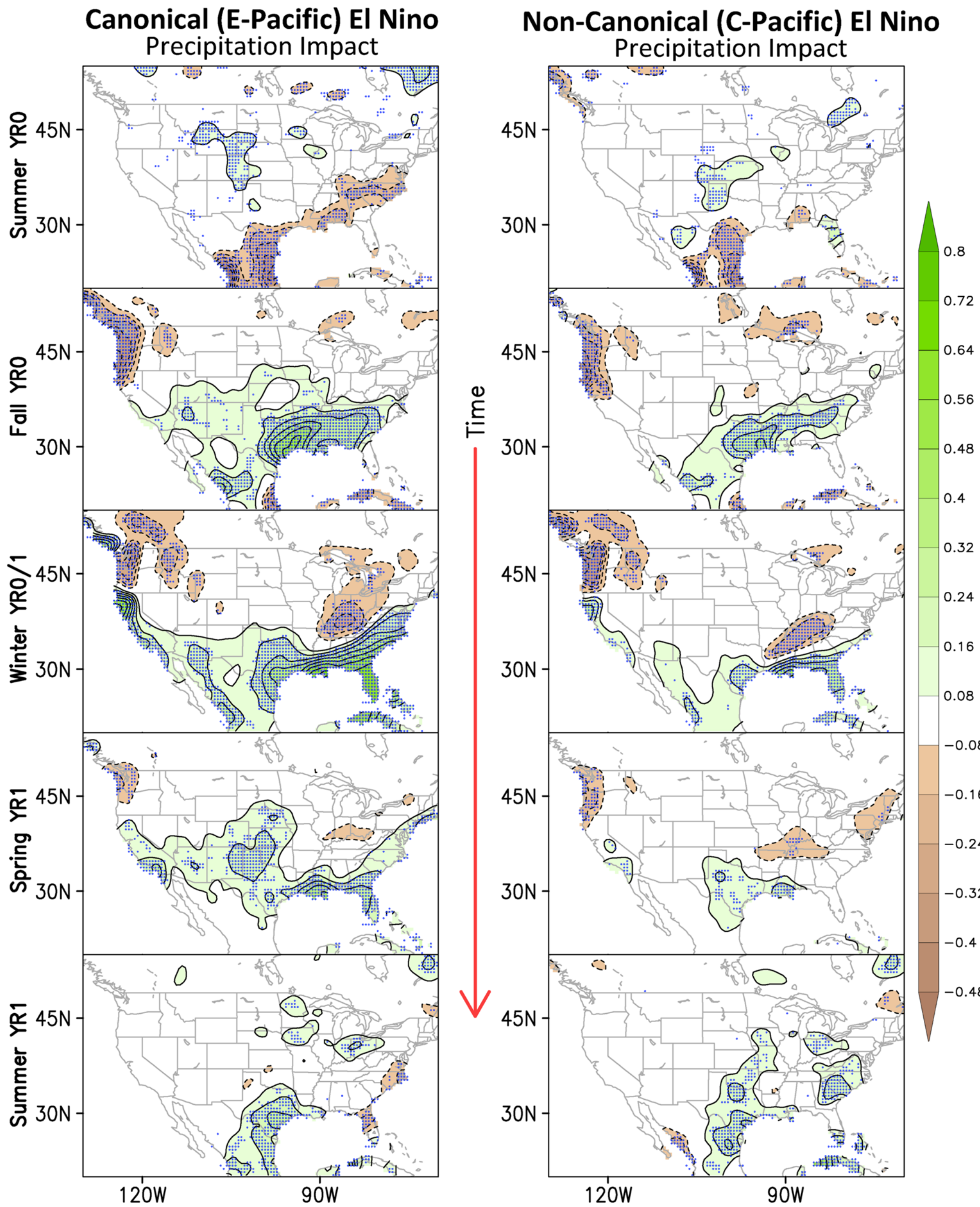

Figure 4. Canonical (East Pacific) and Noncanonical (Central Pacific) El Niño's influence on US precipitation: Lagged regressions on the ENSO-Growth SST PC (which peaks in YR0-Summer, cf. Figure 1) characterize Canonical El Niño's precipitation influence (left), while lead-lag regressions on the Noncanonical ENSO SST PC (which peaks in YR0-Fall) characterize the precipitation influence during Noncanonical El Niño (*aka* Central Pacific El Niño or El Niño Modoki; right). GPCC (v8; 0.5°) precipitation is regressed during 1901–2016 and shown after smoothing (4 × *smth9* in GrADS). Seasonal anomalies are shown from the summer of YR0 (El Niño Growth year) to the summer of YR1 (El Niño Decay year), with time running downward, and contoured/shaded at interval and threshold of 0.08 mm/day/(unit PC). The amplitude of anomalies in a specific season will depend on the ENSO SST PC values in that season. Regressions statistically significant at the 95% confidence level, as assessed by a two-tailed Student's *t* test, are stippled (blue dots). ENSO, El Niño Southern Oscillation; SST, Sea Surface Temperature; GPCC, Global Precipitation Climatology Center; PC, Principal Component.

season. Unlike previous analyses, Figure 4 does not refer to specific El Niño episodes; instead, it shows regressions of precipitation on Canonical and Noncanonical SST PCs over 1901–2016, i.e., the characteristic precipitation anomalies per unit PC-amplitude. The Canonical El Niño's influence (left column) is strongest in winter and structurally similar to the composited El Niño precipitation anomalies shown in Figures 2 and 3, especially the ones reconstructed from the two Canonical SST PCs (Figure 3, right-middle); the latter, not surprisingly. Comparison with Noncanonical El Niño's winter influence (Figure 4, right-middle) reveals interesting regional differences: The increased precipitation signal over northern California is weaker in the Noncanonical case, as are the above-normal precipitation footprints over Southeastern US and the Eastern Seaboard; both broadly consistent with the winter-only analyses of Guo et al. (2017, Figure 9) and Zhang et al. (2020, Figure 3).

The two El Niño types exert different influences in subsequent seasons as well: The above-normal spring precipitation over California and the Gulf Coast is more robust in Canonical El Niño, and the impact on Eastern Seaboard precipitation is oppositely signed during spring and summer.

6. Concluding Remarks

El Niño Southern Oscillation—a leading mode of interannual ocean-atmosphere variability in the tropical Pacific—strongly influences the hydroclimate of adjacent continents. Scoping out El Niño's seasonal influence on North American precipitation—a potentially predictable signal—is the analysis goal. Although key features of the El Niño's influence on winter precipitation are well-known, is the El Niño influence fully scoped out? And in the shoulder seasons of winter, i.e., preceding fall and subsequent spring is it even adequately characterized? Answers are sought from analyses of century-long (1901–2016) SST and precipitation records as realistic representations of regional hydroclimate variability still elude climate system models, at least, of the IPCC-AR5 genre (Sengupta & Nigam, 2019).

The scope of El Nino's influence on North American precipitation is estimated from seasonally stratified composites of the precipitation anomalies observed during four strong recent El Nino episodes. If the extent of El Nino's influence can be so straight-forwardly characterized, what is the purpose of this analysis? Its primary purpose is to assess the efficacy of a commonly used method for characterizing (and predicting) ENSO's influence, one based on linear regressions on the Niño 3.4 SST index—a widely used marker of ENSO variability.

Using El Niño-related composites of North American precipitation anomalies as target, it is shown that El Niño's precipitation influence can be more fully reconstructed from assembling the regressions of precipitation on the four SST principal components (PCs) constituting ENSO variability rather than on an SST index keyed just to El Niño's mature phase (e.g., the Niño 3.4 index)—this, despite the close correspondence (~0.97 correlation) of the observed Niño3.4 SST index with the one constructed from the four ENSO-related SST PCs; for reasons discussed in Section 4.4.

The Niño 3.4 index-based reconstruction of El Niño's influence is shown to be suboptimal in boreal winter when anomaly amplitudes are underestimated by a factor of ~2, and subpar in the seasons following winter when it indicates North America to be devoid of notable precipitation anomalies, in contrast with both PC-based influence and El Niño composites (middle and right columns, Figure 2); the influence reconstruction in even more subpar if based on contemporaneous regressions on the Niño 3.4 index rather than lagged ones on the Niño 3.4 *winter* index.

The seasonal influence of Canonical and Noncanonical El Niño variability on North American precipitation is also characterized both objectively and contextually, i.e., from the same parent analysis (yielding temporally orthonormal PCs but *not* spatially orthogonal patterns), precluding aliasing of precipitation regressions. Noncanonical El Niño's influence is weaker in winter, notably, over northern California and the Eastern Seaboard. The two El Niño types also have opposite-signed impact on Eastern Seaboard precipitation in the following spring and summer—an exploitable difference in the context of seasonal hydroclimate prediction.

We posit that the historical over-reliance on linear regressions on the Niño3.4 SST index (and that too, contemporaneous ones, e.g., NOAA CPC) has underestimated El Niño's hydroclimate influence over North America; the underestimation is modest in boreal winter but severe in its shoulder seasons. The extent of El Niño's influence on precipitation over the Americas is shown to be more substantial than previously recognized and pronounced not just in northern winter but even in its shoulder seasons—enhancing prospects for year-round seasonal prediction.

10.1029/2020GL091447

Appendix:

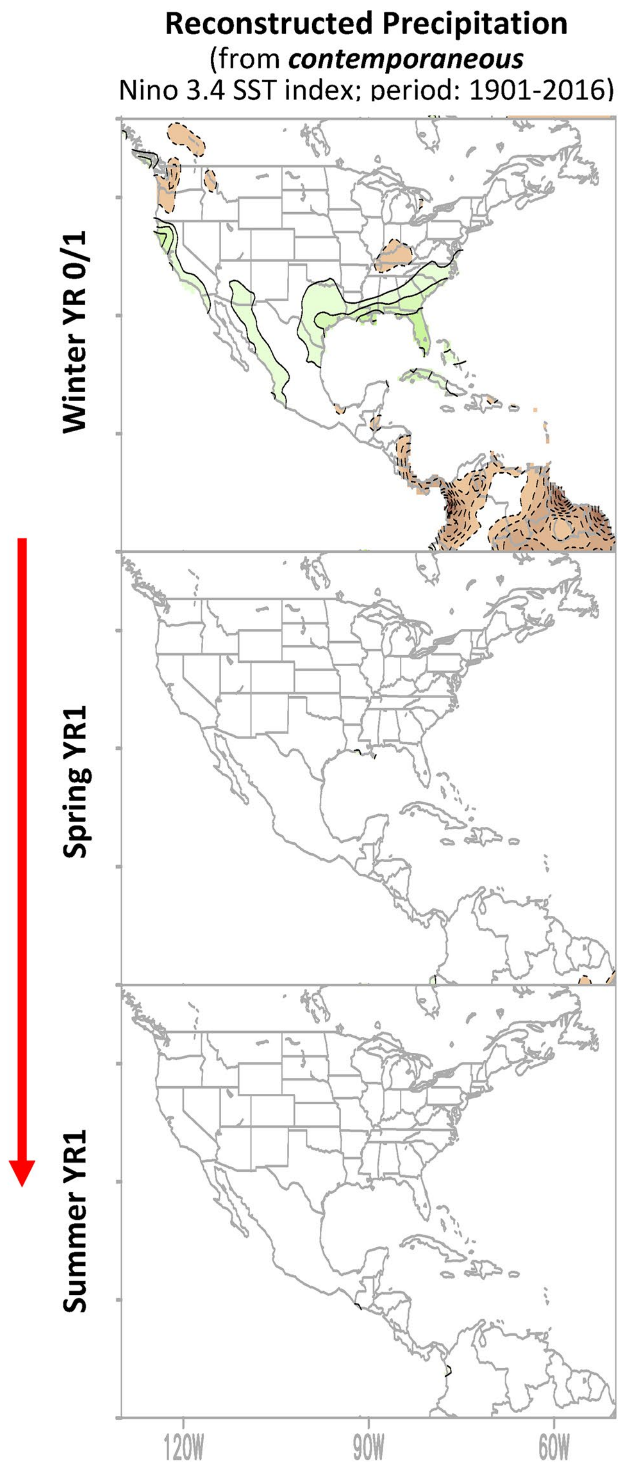

Figure A1. Reconstructed El Niño Precipitation Anomalies over the Americas, composited over four episodes (1972–1973, 1982–1983, 1997–1998, and 2015–2016): Reconstruction from contemporaneous regressions on the Niño 3.4 SST index. GPCC (v8) precipitation is regressed and contoured/shaded at interval and threshold of 0.4 mm/day. Seasonal anomalies are shown from boreal winter to the summer of YR1 (El Nino Decay year), with time running downward. Rest as in Figure 2, including the regression period, 1901–2016.

Data Availability Statement

All datasets analyzed in this study (sea surface temperature, precipitation) are publicly available through online data archives noted in their citation. The global sea surface temperature analysis, especially the resulting principal components—the analysis fulcrum—are available to the research community via the University of Maryland weblink http://dsrs.atmos.umd.edu/DATA/pcs_glsst/.

Acknowledgments

The authors acknowledge the support of the U.S. National Science Foundation through Grant AGS1439940. Agniv Sengupta was additionally supported by India's National Monsoon Mission and the University of Maryland's Graduate School, the latter through the Ann G. Wylie Dissertation Fellowship. Agniv's contribution to the project was completed at the Jet Propulsion Laboratory, California Institute of Technology, under contract with the National Aeronautics and Space Administration.

References

Aceituno, P. (1988). On the functioning of the Southern Oscillation in the South American sector. Part I: Surface climate. *Monthly Weather Review*, *116*(3), 505–524.

Becker, A., Finger, P., Meyer-Christoffer, A., Rudolf, B., Schamm, K., Schneider, U., & Ziese, M. (2013). A description of the global land-surface precipitation data products of the Global Precipitation Climatology Center with sample applications including centennial (trend) analysis from 1901–present. *Earth System Science Data*, *5*(1), 71–99.

Capotondi, A., Wittenberg, A. T., Newman, M., di Lorenzo, E., Yu, J. Y., Braconnot, P., et al. (2015). Understanding ENSO diversity. *Bulletin of the American Meteorological Society*, *96*(6), 921–938.

Compo, G. P., & Sardeshmukh, P. D. (2010). Removing ENSO-related variations from the climate record. *Journal of Climate*, *23*(8), 1957–1978.

Guan, B., & Nigam, S. (2008). Pacific sea surface temperatures in the twentieth century: An evolution-centric analysis of variability and trend. *Journal of Climate*, *21*(12), 2790–2809.

Guan, B., & Nigam, S. (2009). Analysis of Atlantic SST variability factoring interbasin links and the secular trend: Clarified structure of the Atlantic Multidecadal Oscillation. *Journal of Climate*, *22*(15), 4228–4240.

Guo, Y., Ting, M., Wen, Z., & Lee, D. E. (2017). Distinct patterns of tropical Pacific SST anomaly and their impacts on North American climate. *Journal of Climate*, *30*, 5221–5240.

Infanti, J. M., & Kirtman, B. P. (2016). North American rainfall and temperature prediction response to the diversity of ENSO. *Climate Dynamics*, *46*, 3007–3023.

Joseph, R., & Nigam, S. (2006). ENSO evolution and teleconnections in IPCC's twentieth-century climate simulations: Realistic representation?. *Journal of Climate*, *19*(17), 4360–4377.

Kao, H. Y., & Yu, J. Y. (2009). Contrasting eastern-Pacific and central-Pacific types of ENSO. *Journal of Climate*, *22*(3), 615–632.

Nigam, S. (2003). *Teleconnections*. In J. R. Holton, J. A. Pyle, & J. A. Curry (Eds.), Encyclopedia of atmospheric sciences (pp. 2243–2269). London: Academic Press.

Nigam, S., & Baxter, S. (2015). *Teleconnections*. In G. North, F. Zhang, & J. Pyle (Eds.), Encyclopedia of atmospheric sciences (2nd ed., pp. 90–109). London: Academic Press.

Nigam, S., & Ruiz-Barradas, A. (2006). Seasonal hydroclimate variability over North America in global and regional reanalyzes and AMIP simulations: Varied representation. *Journal of Climate*, *19*, 815–837.

Nigam, S., Sengupta, A., & Ruiz-Barradas, A. (2020). Atlantic-Pacific links in observed multidecadal SST variability: Is Atlantic multidecadal oscillation's phase-reversal orchestrated by Pacific decadal oscillation?. *Journal of Climate*, *33*, 5479–5505.

NOAA Climate Prediction Center. *Global ENSO temperature and precipitation linear regressions*. Retrieved from https://www.cpc.ncep.noaa.gov/products/precip/CWlink/ENSO/regressions/

Rasmusson, E. M., & Carpenter, T. H. (1983). The relationship between eastern equatorial Pacific sea surface temperatures and rainfall over India and Sri Lanka. *Monthly Weather Review*, *111*(3), 517–528.

Rayner, N. A., Parker, D. E., Horton, E. B., Folland, C. K., Alexander, L. V., Rowell, D. P., et al. (2003). Global analyses of sea surface temperature, sea ice, and night marine air temperature since the late nineteenth century. *Journal of Geophysical Research: Atmospheres*, *108*, 4407. https://doi.org/10.1029/2002JD002670

Ropelewski, C. F., & Halpert, M. S. (1987). Global and regional scale precipitation patterns associated with the El Niño/Southern Oscillation. *Monthly Weather Review*, *115*(8), 1606–1626.

Sengupta, A., & Nigam, S. (2019). The Northeast Winter Monsoon over the Indian Subcontinent and Southeast Asia: Evolution, Interannual Variability, and Model Simulations. *Journal of Climate*, *32*(1), 231–248.

Trenberth, K. E., Branstator, G. W., Karoly, D., Kumar, A., Lau, N. C., & Ropelewski, C. (1998). Progress during TOGA in understanding and modeling global teleconnections associated with tropical sea surface temperatures. *Journal of Geophysical Research*, *103*(C7), 14291–14324.

Zhang, T., Hoerling, M. P., Hoell, A., Perlwitz, J., & Eischeid, J. (2020). Confirmation for and predictability of distinct U.S. Impacts of El Niño flavors. *Journal of Climate*, *33*, 5971–5991.